Electronic Supplementary Material (ESI) for Inorganic Chemistry Frontiers.

Supporting information for the paper:

Structural transformation of metal-organic frameworks and identification of electrocatalytically active species during the oxygen evolution reaction under neutral condition

Xiaoqiang Liang,[a] Sen Wang,[a] Jingyu Feng,*[b,e] Zhen Xu,[b,f] Zhenyu Guo,[b] Hui Luo,[b] Feng Zhang,[d] Wen Chen,[c] Lei Feng,[c] Chengan Wan[c] and Maria-Magdalena Titirici*[b]

[a] *School of Environmental and Chemical Engineering, Xi'an Polytechnic University, 710048, Xi'an, PR China*

[b] *Department of Chemical Engineering, Imperial College London, South Kensington Campus, SW7 2AZ, London, UK. E-mail: j.feng19@imperial.ac.uk, m.titirici@imperial.ac.uk*

[c] *Beijing Spacecrafts, 100094, Beijing, PR China*

[d] *Key Laboratory of Photochemical Biomaterials and Energy Storage Materials, Heilongjiang Province and College of Chemistry and Chemical Engineering, Harbin Normal University, Harbin 150025, PR China*

[e] *School of Engineering and Materials Science, Queen Mary university of London, E1 4NS, London, UK*

[f] *Yusuf Hamied Department of Chemistry, University of Cambridge, CB2 1EW, Cambridge, UK*

Table of Contents

I. Crystallographic data and structures

Table S1 Crystallographic data and details of refinements for **Co-Ci-2D**, **Ni-Ci-2D** and **Co-Ci-mono-A**.

Compounds	**Co-Ci-2D**	**Ni-Ci-2D**	**Co-Ci-mono-A**
Empirical formula	$C_{11}H_{14}N_3O_4Co_{0.50}$	$C_{11}H_{14}N_3O_4Ni_{0.50}$	$C_{16}H_{18}N_4O_8Co$
*M*r	281.72	281.61	453.27
Crystal system	Monoclinic	Monoclinic	Orthorhombic
Space group	$P2_1/n$	$P2_1/n$	*Pbca*
a (Å)	6.5965(9)	6.5606(4)	6.8341(4)
b (Å)	18.185(3)	18.0108(13)	13.4050(9)
c (Å)	10.8523(18)	10.9601(8)	19.5832(13)
α (°)	90	90	90
β (°)	93.924(5)	93.960(2)	90
γ (°)	90	90	90
V (Å^3)	1298.8(4)	1291.97(15)	1794.0(2)
Z	4	4	4
D_c (g cm^{-3})	1.441	1.448	1.678
μ(mm^{-1})	0.717	0.808	1.013
F(000)	586	588	932
θ range [º]	2.9−26.4	2.3−26.4	3.0−26.4
Collected reflections	20025	20355	20650
Unique reflections	2638	2644	1833
Parameters	177	171	149
T (K)	150	150	150
R_1 [a], wR_2 [b] [I > 2σ (I)]	0.0470, 0.0969	0.0330, 0.0884	0.0341, 0.0782
R_1 [a], wR_2 [b] [all data]	0.0846，0.1135	0.0474, 0.0884	0.0506, 0.0876
GOF	1.033	1.027	1.071
Largest peak and hole (e ·Å^{-3})	0.42, −0.34	0.27, −0.24	0.35, −0.45

[a] $R_1 = \sum||F_o|-|F_c||/\sum|F_o|$. [b] $wR_2 = [\sum w(|F_o^2|-|F_c^2|)^2/\sum w(|F_o^2|)^2]^{1/2}$.

Table S2 Selected bond lengths (Å) and angles (°) for **Co-Ci-2D**, **Ni-Ci-2D** and **Co-Ci-mono-A**.

		Co-Ci-2D	
Co(1)−O(1a)	2.083(2)	Co(1)−O(1b)	2.083(2)
Co(1)−O(3)	2.097(2)	Co(1)−O(3c)	2.097(2)
Co(1)−N(2)	2.138(3)	Co(1)−N(2c)	2.138(3)
O(1a)−Co(1)−O(3)	90.94(8)	O(1a)−Co(1)−N(2)	93.19(9)
O(1a)−Co(1)−O(3c)	89.07(8)	O(1a)−Co(1)−N(2c)	86.81(9)
O(1a)−Co(1)−O(1b)	180.00	O(1b)−Co(1)−N(2)	86.81(9)
O(1b)−Co(1)−O(3)	89.07(8)	O(1b)−Co(1)−O(3c)	90.94(8)
O(1b)−Co(1)−N(2c)	93.19(9)	O(3)−Co(1)−N(2)	87.02(10)
O(3)−Co(1)−O(3c)	180.00	O(3)−Co(1)−N(2c)	92.98(10)
O(3c)−Co(1)−N(2)	92.98(10)	O(3c)−Co(1)−N(1c)	86.81(9)
N(2)−Co(1)−N(2c)	180.00		
		Ni-Ci-2D	
Ni(1)−O(2a)	2.0711(14)	Ni(1)−O(2b)	2.0711(14)
Ni(1)−O(3)	2.0566(13)	Ni(1)−O(3c)	2.0566(13)
Ni(1)−N(1)	2.0887(18)	Ni(1)−N(1c)	2.0887(18)
O(2a)−Ni(1)−O(3)	92.06(5)	O(2a)−Ni(1)−N(1)	93.11(6)
O(2a)−Ni(1)−O(3c)	87.94(5)	O(2a)−Ni(1)−N(1c)	86.89(6)
O(2a)−Ni(1)−O(2b)	180.00	O(2b)−Ni(1)−O(3)	87.94(5)
O(2b)−Ni(1)−N(1)	86.89(6)	O(2b)−Ni(1)−O(3c)	92.06(5)
O(2b)−Ni(1)−N(1c)	93.11(6)	O(3)−Ni(1)−N(1)	87.08(7)
O(3)−Ni(1)−O(3c)	180.00	O(3)−Ni(1)−N(1c)	92.92(7)
O(3c)−Ni(1)−N(1)	92.92(7)	O(3c)−Ni(1)−N(1c)	87.08(7)
N(1)−Ni(1)−N(1c)	180.00		
		Co-Ci-mono-A	
Co(1)−O(3)	2.100(2)	Co(1)−O(3a)	2.100(2)
Co(1)−O(4)	2.1106(19)	Co(1)−O(4a)	2.1106(19)
Co(1)−N(1)	2.141(2)	Co(1)−N(1a)	2.141(2)
O(3)−Co(1)−O(4)	88.18(7)	O(3)−Co(1)−N(1)	89.79(8)
O(3)−Co(1)−O(3a)	180.00	O(3)−Co(1)−O(4a)	91.83(7)
O(3)−Co(1)−N(1a)	90.21(8)	O(4)−Co(1)−N(1)	87.91(7)
O(3a)−Co(1)−O(4)	91.83(7)	O(4)−Co(1)−O(4a)	180.00
O(4)−Co(1)−N(1a)	92.09(7)	O(3a)−Co(1)−N(1)	90.21(8)
O(4a)−Co(1)−N(1)	92.09(7)	N(1)−Co(1)−N(1a)	180.00
O(3a)−Co(1)−O(4a)	88.18(7)	O(3a)−Co(1)−N(1a)	89.79(8)
O(4a)−Co(1)−N(1a)	87.91(7)		

Symmetry codes : a) 1/2−*x*, 1/2+*y*, 1/2−*z*; b) −1/2+*x*, 3/2−*y*, −1/2+*z*; c) −*x*, 2−*y*, −*z* for **Co-Ci-2D**; a) 1/2−*x*, 1/2+*y*, 1/2−*z*; b) −1/2+*x*, 3/2−*y*, −1/2+*z*; c) −*x*, 2−*y*, −*z* for **Ni-Ci-2D**; a) 2−*x*, 2−*y*, −*z* for **Co-Ci-mono-A**.

Table S3 Hydrogen−bonding geometry parameters (Å, °) for **Co-Ci-2D**, **Ni-Ci-2D** and **Co-Ci-mono-A**.

D−H···A	d(D−H)	d(H···A)	d(D···A)	∠(DHA)
		Co-Ci-2D		
O(3)−H(3WA)···O(2a)	0.86(4)	1.81(4)	2.632(3)	159(3)
O(3)−H(3WA)···O(4d)	0.82(4)	1.92(4)	2.727(3)	168(3)
N(1)−H(1A)···O(3)	0.88	2.33	2.859(4)	119
N(1)−H(1A)···O(2e)	0.88	2.00	2.792(3)	149
		Ni-Ci-2D		
O(3)−H(3WA)···O(1a)	0.84	1.86	2.618(2)	148
O(3)−H(3WA)···O(4d)	0.88	1.87	2.734(2)	166
N(2)−H(2)···O(3)	0.88	2.29	2.806(2)	118
N(2)−H(2)···O(1d)	0.88	2.01	2.799(2)	149
		Co-Ci-mono-A		
O(3)−H(3WB)···O(1b)	0.77(3)	2.07(3)	2.779(2)	154(3)
O(3)−H(3WA)···O(2c)	0.78(4)	1.94(4)	2.695(2)	164(4)
O(3)−H(4WA)···O(1d)	0.75(4)	2.00(4)	2.739(2)	170(4)
O(4)−H(4WB)···O(1c)	0.89(4)	1.91(4)	2.801(2)	172(3)
N(2)−H(2)···O(2c)	0.88	1.94	2.773(3)	156

Symmetry codes: a) 1/2−*x*,1/2+*y*,1/2−*z*; d) 1−*x*,2−*y*, −*z*; e) 1/2+*x*,3/2−*y*, −1/2+*z* for **Co-Ci-2D**; a) 1/2−*x*,1/2+*y*,1/2−*z*; d) 1/2+*x*, 3/2−*y*, −1/2+*z* for **Ni-Ci-2D**; a) 1−*x*, 1−*y*, 1−*z*; b) 5/2−*x*, 2−*y*, −1/2+*z*; c)2−*x*, 1/2+*y*, 1/2−*z*; d) 3/2−*x*, 2−*y*, −1/2+*z* for **Co-Ci mono-A**.

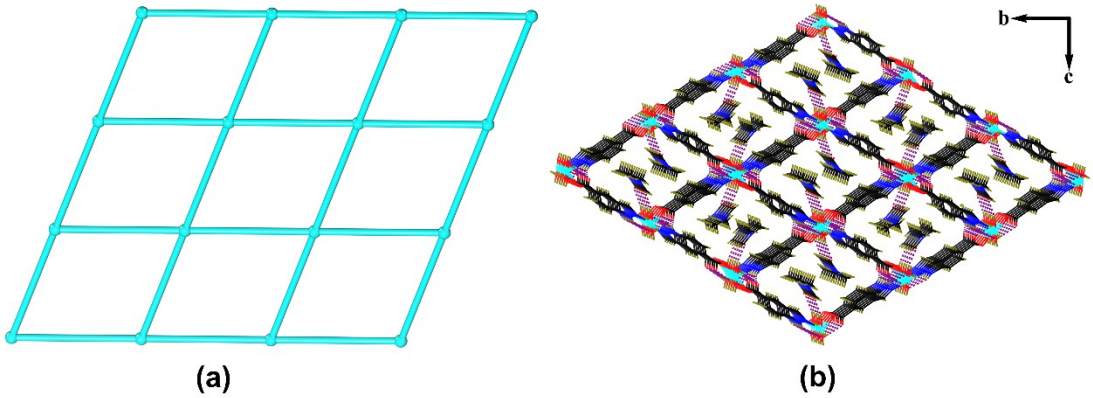

Fig. S1 (a) A 2D metal-organic framework with (4, 4) topology in **Co-Ci-2D**. (b) The cavity was occupied by DMF molecules and the related hydrogen-bonding interactions in **Co-Ci-2D**.

II. Infrared absorption spectra of Co-Ci-2D and Ni-Ci-2D

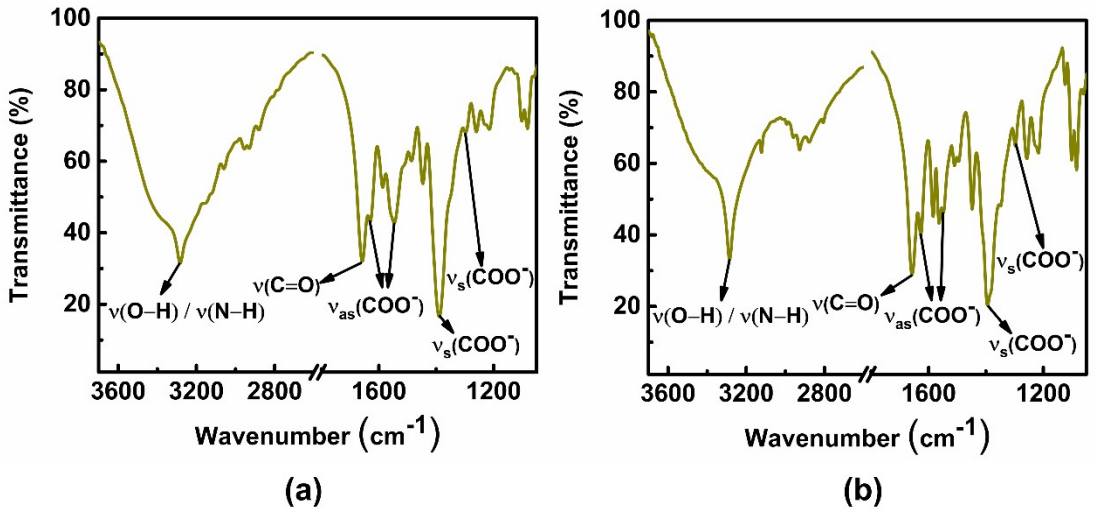

Fig. S2 IR absorption spectra of **Co-Ci-2D** (a) **and Ni-Ci-2D** (b) in the solid state at room temperature.

III. Thermogravimetric analysis curves of Co-Ci-2D and Ni-Ci-2D

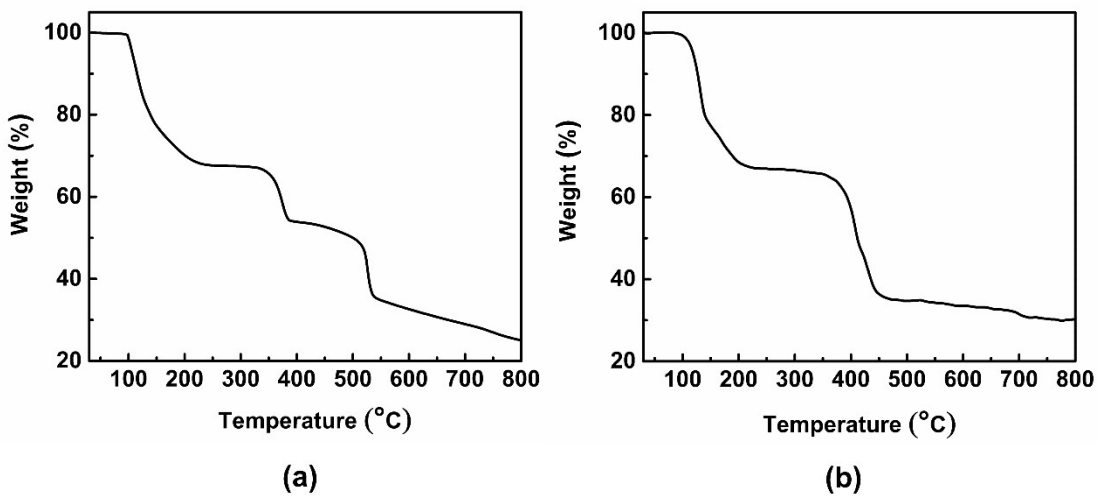

Fig. S3 (a) Thermogravimetric curves for **Co-Ci-2D** (a) **and Ni-Ci-2D** (b).

IV. Linear fitting plots of BET surface area of Co-Ci-2D and Ni-Ci-2D

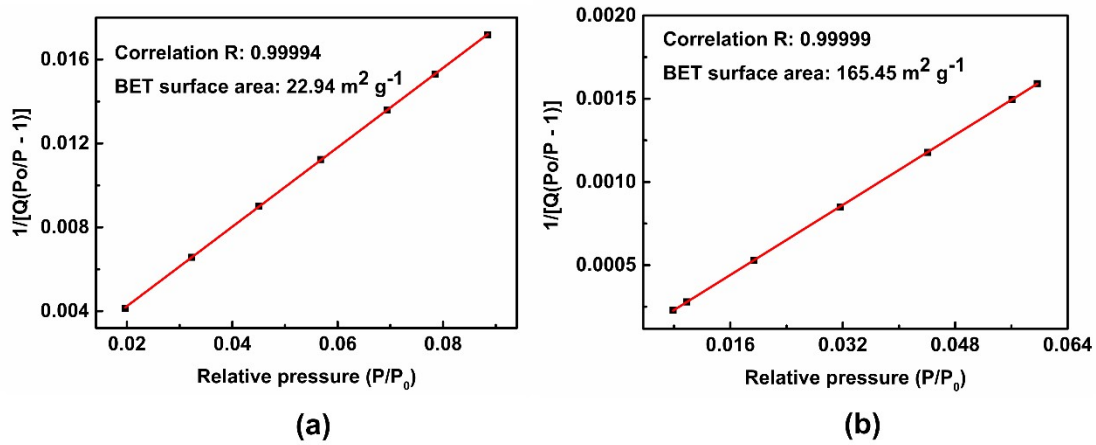

Fig. S4 BET surface area plots calculated from isothermals of **Co-Ci-2D** (a) and **Ni-Ci-2D** (b).

V. Electrochemistry

· OER polarization curves

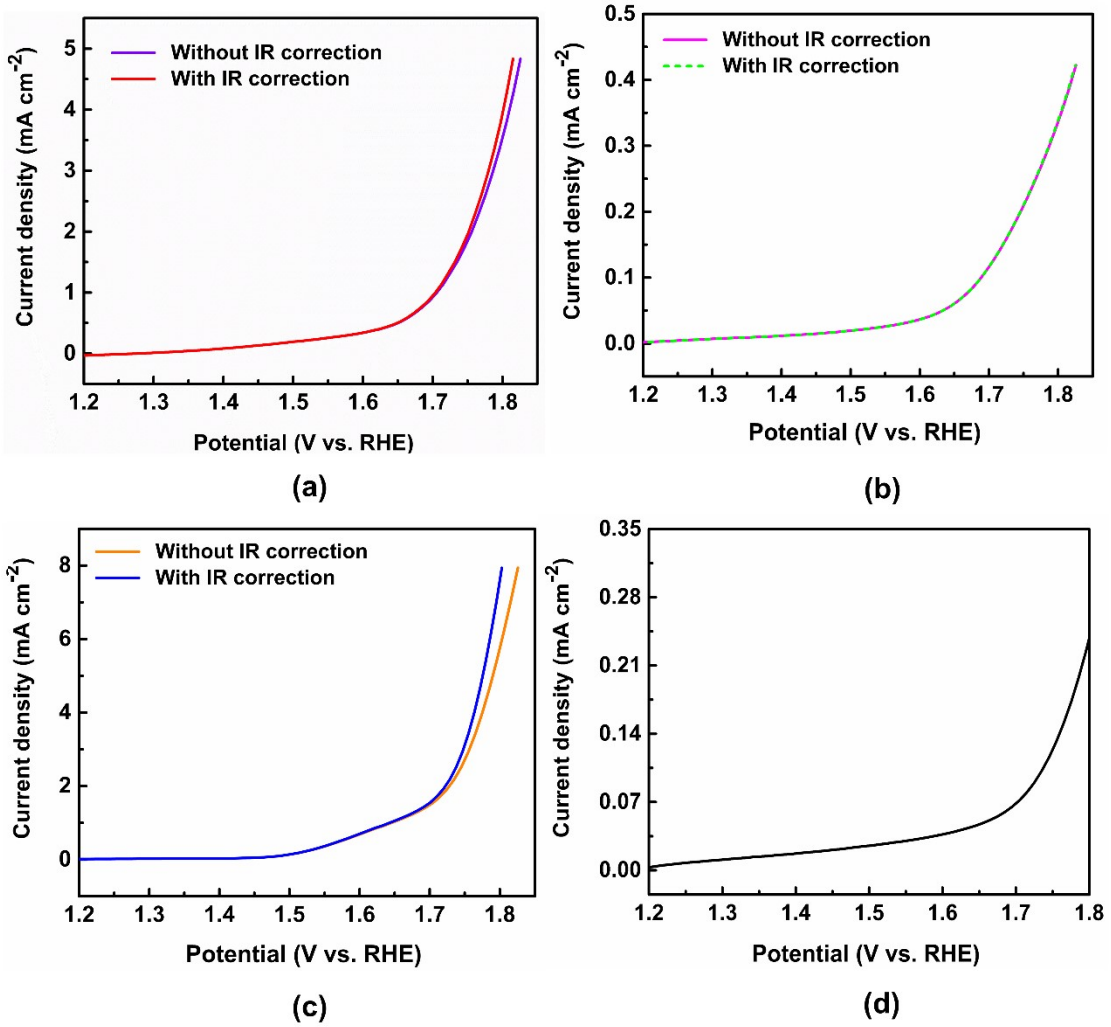

Fig. S5 OER polarization curves of **Co-Ci-2D** (a), **Ni-Ci-2D** (b) and **IrO_2** (c) without and with the IR correction. (d) OER polarization curve of **carbon black (CB)**.

Bare CB shows a very poor OER activity with a current density of 0.25 mA cm^{-2} at 1.8V, indicating the absence of OER activity. Thus, carbon black serves as a conductive additive to improve their conductivities of MOF materials.

· **Cyclic voltammetry**

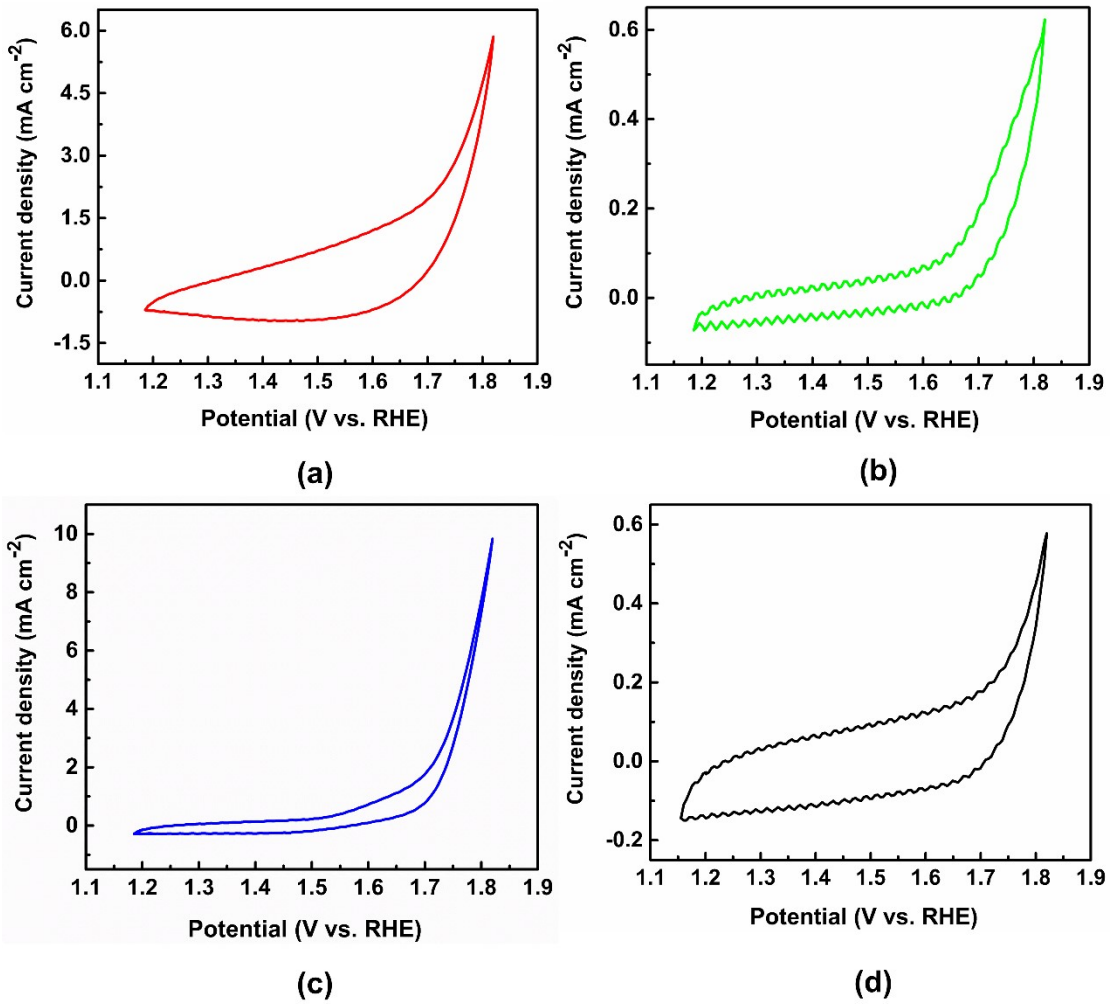

Fig. S6 Cyclic voltametric plots of **Co-Ci-2D** (a), **Ni-Ci-2D** (b), **IrO_2** (c) and **carbon black (CB)** (d) with a sweep rate of 10 mV s^{-1}.

· **Cyclic voltammetry at different scan rates**

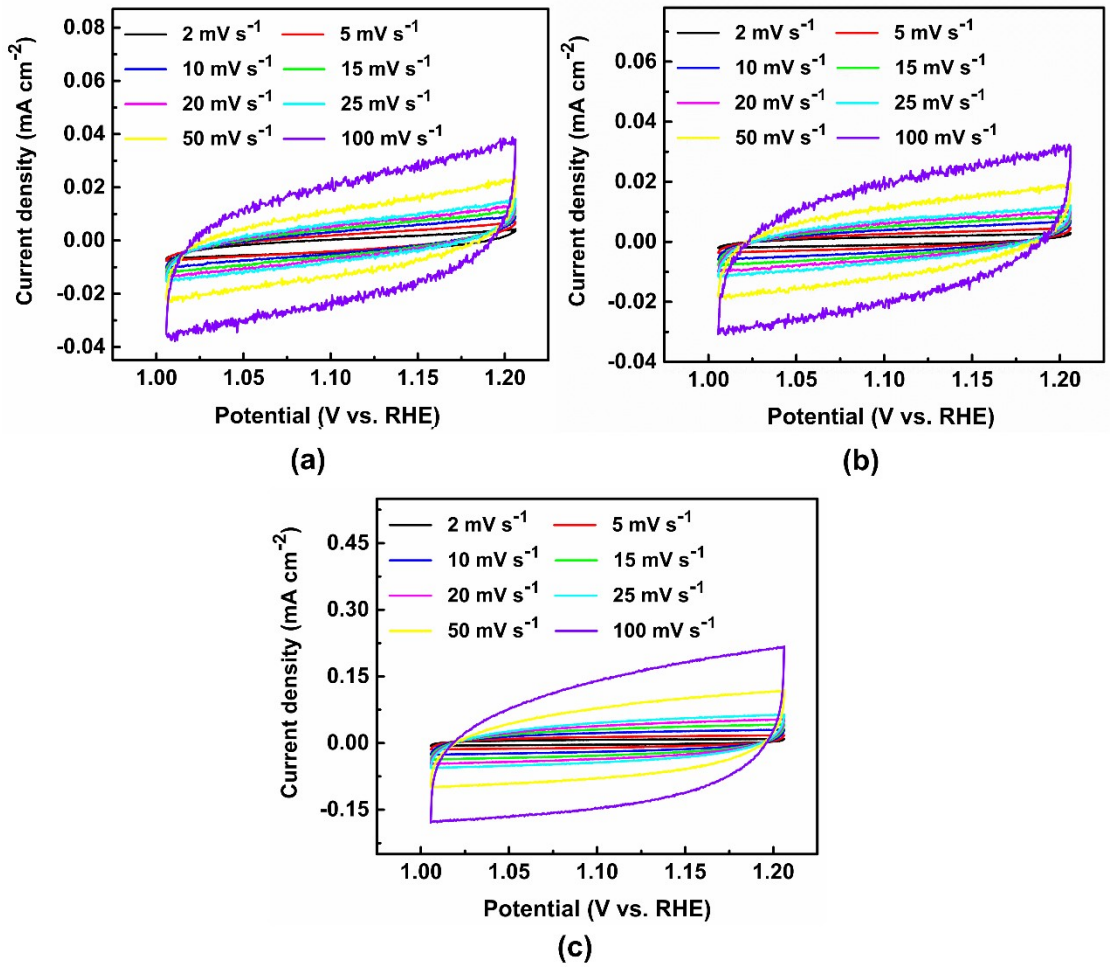

Fig. S7 Cyclic voltametric curves of **Co-Ci-2D** (a), **Ni-Ci-2D** (b) and **IrO_2** (c) at different sweep rates in 0.1 M PBS solution in the non-Faradaic region.

· **Electrochemically active surface area (ECSA)**

Double layer capacitance (C_{dl}) can be calculated by plotting of $\Delta j = (j_a - j_c)/2$ as function of sweep scan rates v in the non-faradaic region:

$$C_{dl} = \frac{\Delta j}{v}$$

The electrochemically active surface area (ECSA) and the normalized current density for the measured samples in 0.1 M phosphate buffer saline can be computed through the following equations, respectively:

$$ECSA = \frac{C_{dl-sample}}{C_{dl-glassy\ carbon}}$$

$$j_{ECSA\text{-}normalized} = \frac{j}{ECSA}$$

Where $C_{dl\text{-}sample}$ is the double layer capacitance of the measured samples, $C_{dl\text{-}glassy\ carbon}$ is the double layer capacitance of the glassy carbon electrode, and j is the current density. In this study, the specific capacitance of $C_{dl\text{-}glassy\ carbon}$ = 178.92 μF cm^{-2} was used according to the typical reported value.[1]

· **Turnover frequency (TOF)**

The TOF value for OER is calculated via the following equation:

$$TOF = \frac{j \times M}{4 \times F \times m}$$

Where j stands for the current density (mA cm^{-2}) at a given overpotential, M is the molecular weight of the catalyst (g mol^{-1}), the number 4 means four moles of electrons per mole of O_2, F represents the faradic constant (96485 C mol^{-1}), and m is the mass loading of the catalyst on the electrode (mg cm^{-2}).

· **Impedance measurements**

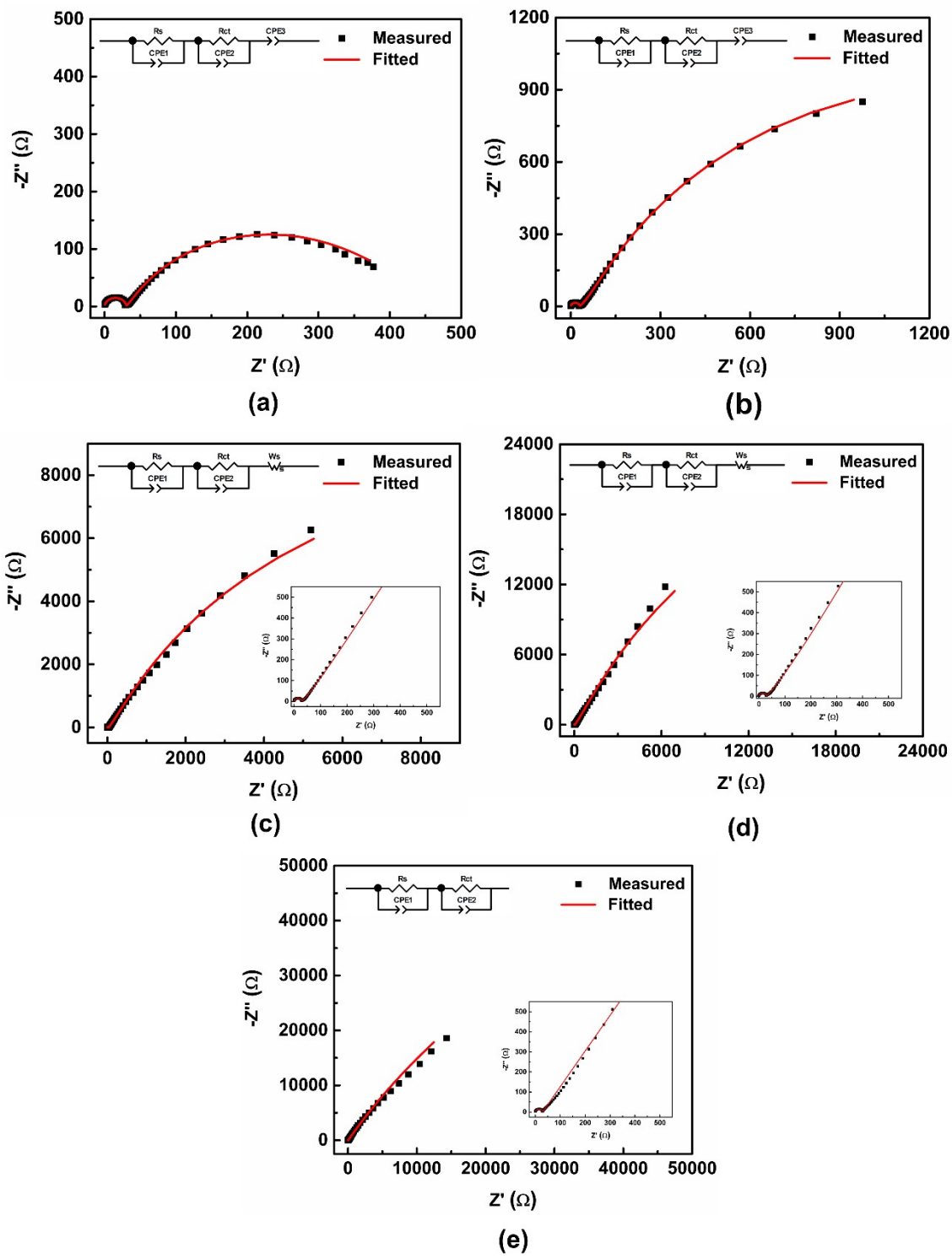

Fig. S8 Nyquist plots and the equivalent circuits for fitting of **Co-Ci-2D** at

overpotentials of 0.53 V (a), 0.43 V (b), 0.33 V (c), 0.23 V (d) and 0.13 V(e) vs. RHE.

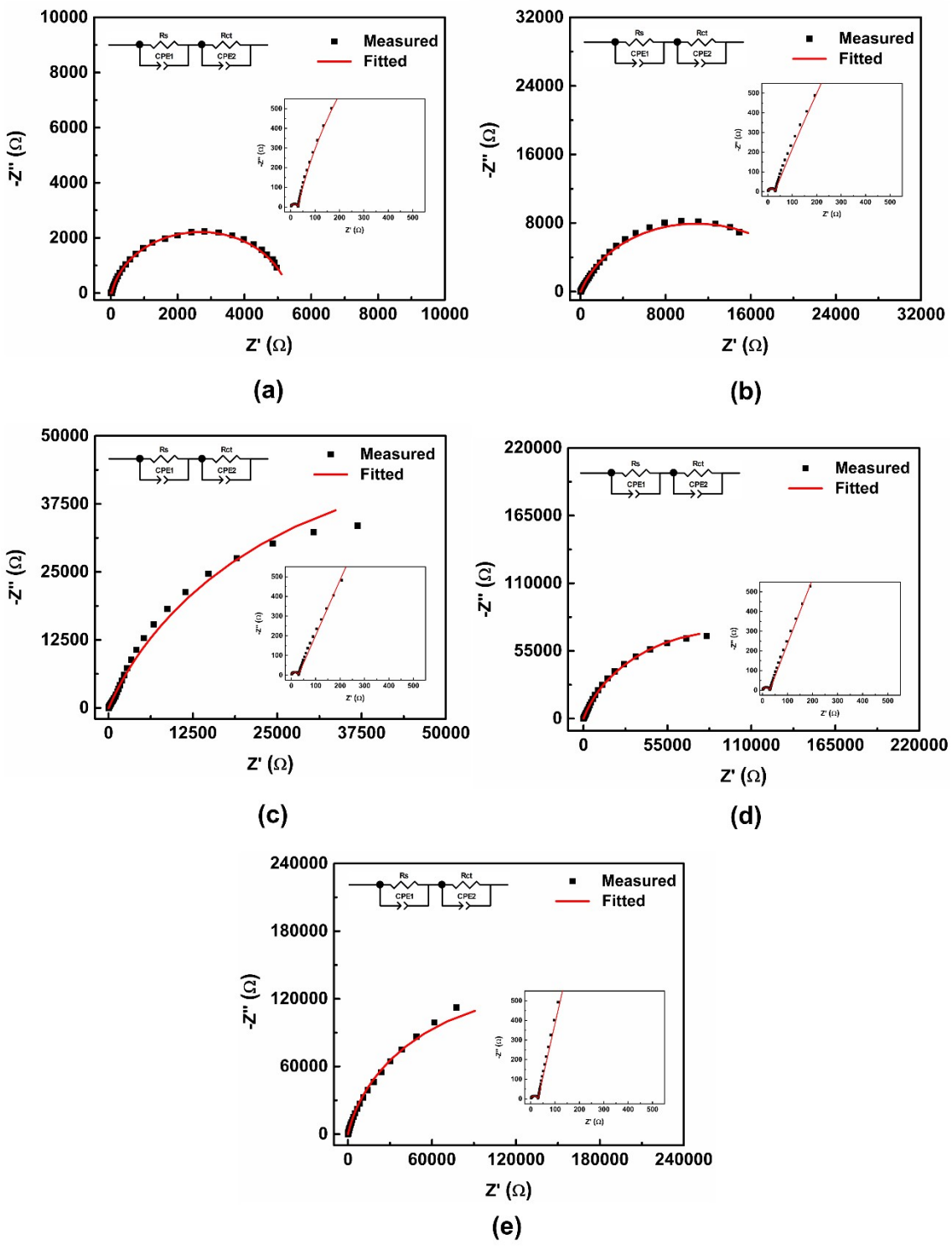

Fig. S9 Nyquist plots and the equivalent circuits for fitting of **Ni-Ci-2D** at

overpotentials of 0.53 V (a), 0.43 V (b), 0.33 V (c), 0.23 V (d) and 0.13 V(e) vs. RHE.

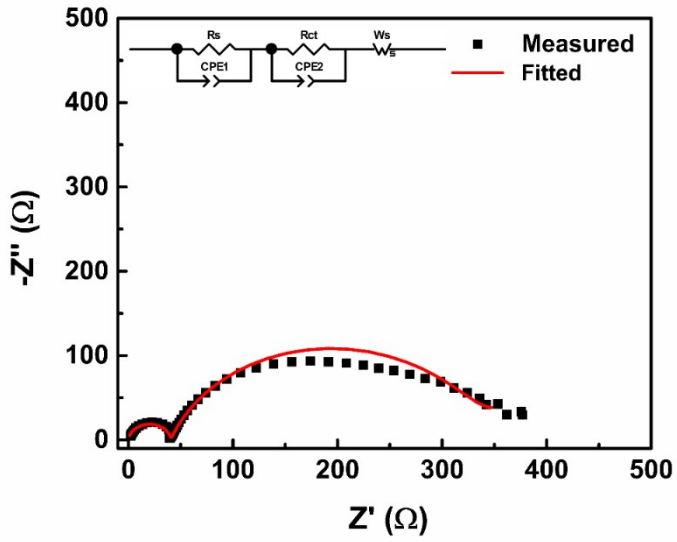

Fig. S10 Nyquist plots and the equivalent circuit for fitting of $\mathbf{IrO_2}$ at an overpotential of 0.53 V vs. RHE.

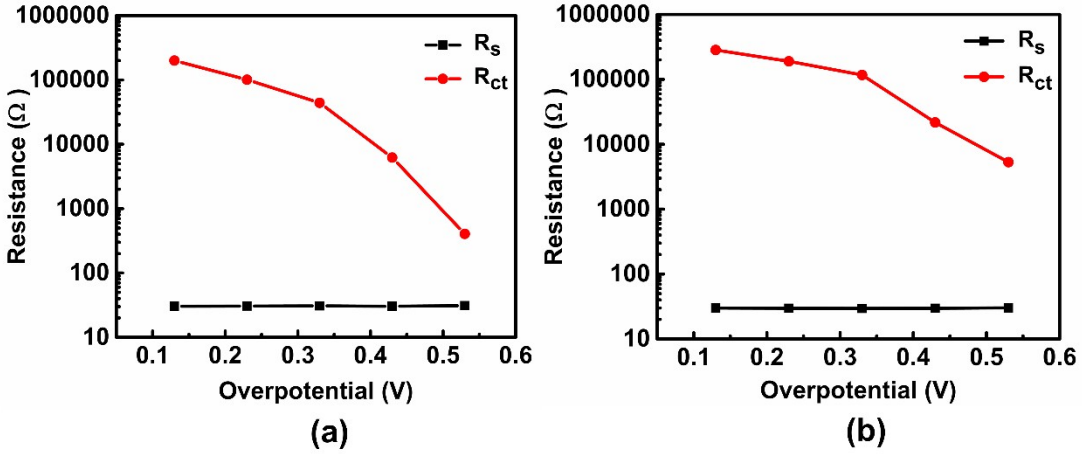

Fig. S11 (a) R_s and R_{ct} of Co-Ci-2D under different overpotentials. (b) R_s and R_{ct} of Ni-Ci-2D under different overpotentials.

Nyquist plots of Co-Ci-2D, Ni-Ci-2D and IrO_2 at different overpotentials are shown in Fig. S8-S10. The low-frequency semicircles stem from the ionic transport resistance through the solution (R_s) and the high-frequency semicircles could be related to the charge transfer resistance (R_{ct}).[2] The principal elements like resistance (R_s and R_{ct}) along with constant phase element (CPE) and Warburg diffuse element (W_s) were selected to fit their Nyquist plots by using the equivalent circuit. As shown in Fig. S11a, the R_s values of Co-Ci-2D were estimated to be 30.40, 30.61, 30.76, 30.34 and 31.08 Ω from the fitting model under the overpotentials of 0.13, 0.23, 0.33, 0.43 and 0.53 V, respectively. Meanwhile, the obtained values of R_{ct} are 2.00×10^5, 1.01×10^5, 4.81×10^4, 6.22×10^3 and 4.05×10^2 Ω, respectively. Ni-Ci-2D yields the R_s values of 29.99, 29.66, 29.54, 29.68 and 30.14 Ω at the overpotentials of 0.13, 0.23, 0.33, 0.43 and 0.53 V, respectively, the corresponding values of R_{ct} reach 2.83×10^5, 1.98×10^5, 1.17×10^5, 2.17×10^4 and 5.30×10^3 Ω, respectively (Fig. S11b). Based on the above data, one can see that there is no obvious alteration of R_s for Co-Ci-2D and Ni-Ci-2D with increasing overpotential, but R_{ct} exhibits a marked reduction in both compounds. It showed that the overpotential had a considerable impact on the charge

transfer resistance of the electrocatalyst, while the ionic transport resistance of the electrolyte is scarcely affected by it. That is to say, the charge transfer resistance is dominant in the reaction of OER relative to the ionic transport resistance of the electrolyte in the measured system.[2] Furthermore, a smaller R_{ct} could trigger a faster charge transfer due to a negative correlation between charge transfer resistance and reaction kinetics. Thus, the difficulty of OER reaction can be determined by comparing the R_{ct} values of the tested samples.

VI. Characterization of Co-Ci-mono-A

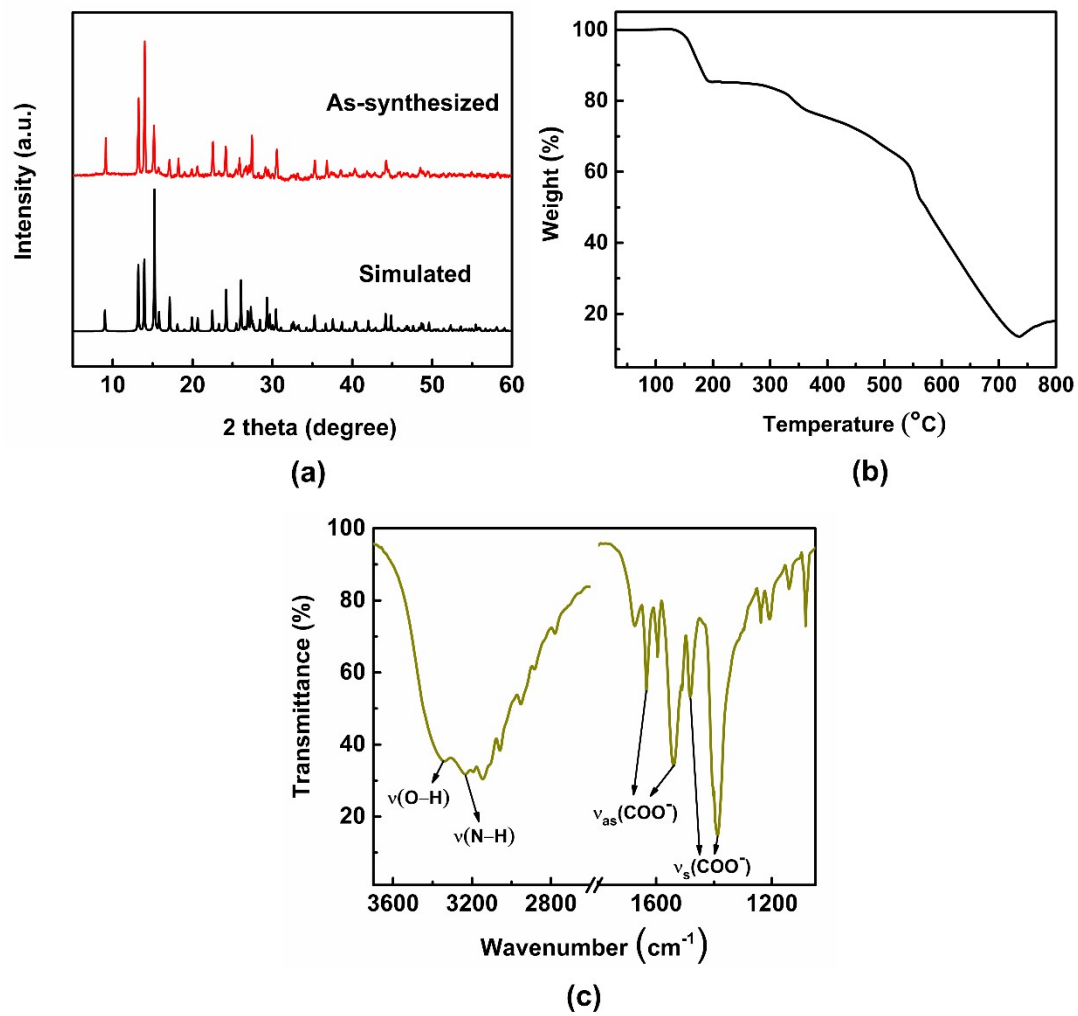

Fig. S12 Structural characterization of **Co-Ci-mono-A**. (a) The PXRD patterns for **Co-Ci-mono-A** of a simulation based on single-crystal analysis and as-synthesized bulk crystals. (b) Thermogravimetric curve for **Co-Ci-mono-A**. (c) IR absorption spectrum of **Co-Ci-mono-A** in the solid state at room temperature.

VII. Characterization of Co-Ci-2D and Ni-Ci-2D soaked in water

· **PXRD patterns**

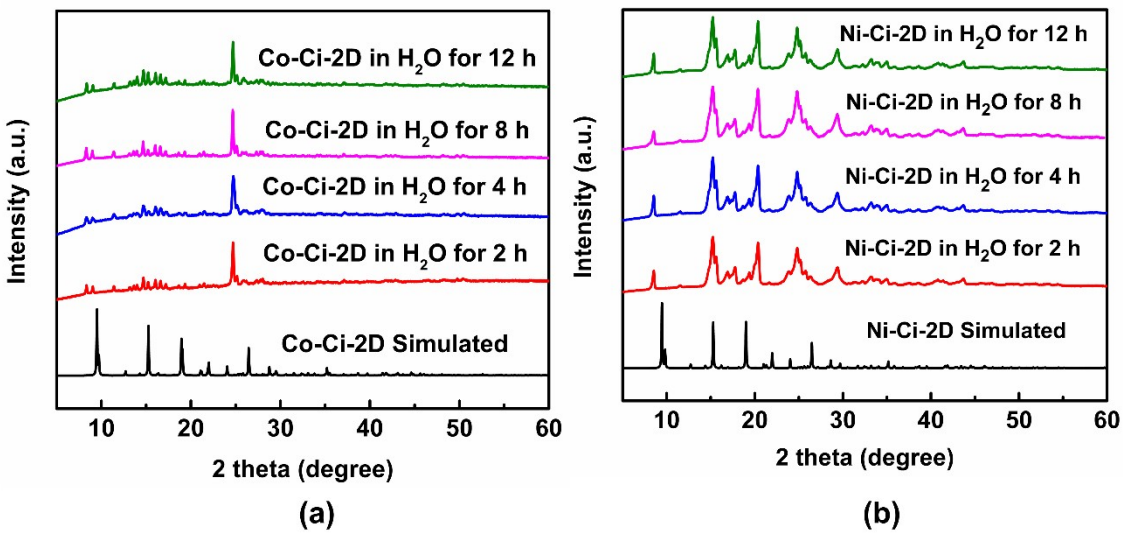

Fig. S13 (a) The PXRD patterns for **Co-Ci-2D** of a simulation based on single-crystal analysis and for **Co-Ci-2D** soaked in water for 2 h, 4 h, 8 h, and 12 h. (b) The PXRD patterns for **Ni-Ci-2D** of a simulation based on single-crystal analysis and for **Ni-Ci-2D** soaked in water for 2 h, 4 h, 8 h, and 12 h.

For Co-Ci-2D samples soaked in water for 2 h, 4 h, 8 h, and 12 h, their PXRD patterns are almost identical characteristic peaks, indicating the presence of the analogical structures and compositions in these samples.

Like all Co-Ci-2D samples soaked in water, all water-treated Ni-Ci-2D samples also show the very similar PXRD patterns, signifying that they have the analogous structures and compositions.

· **TGA curves**

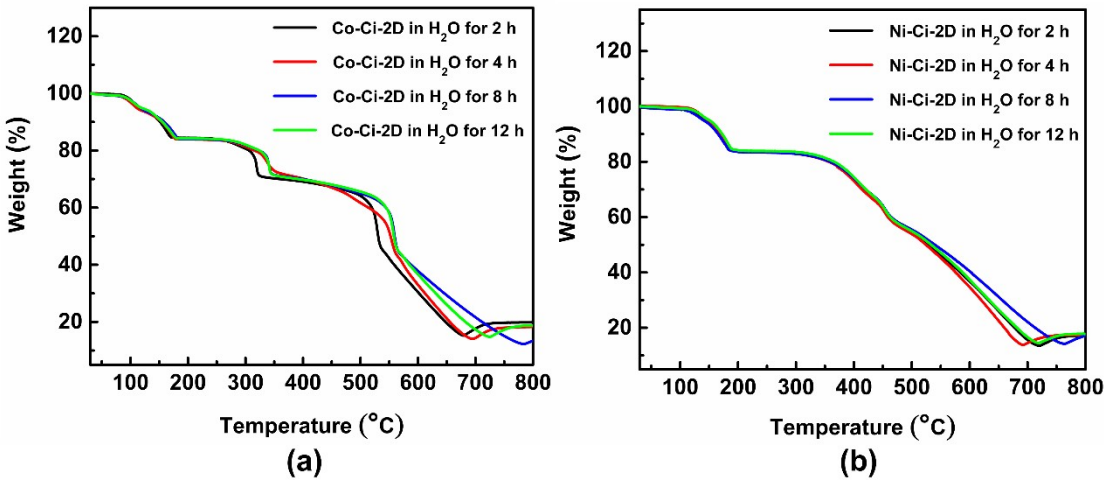

Fig. S14 Thermogravimetric curves for **Co-Ci-2D** (a) and **Ni-Ci-2D** (b) soaked in water for 2 h, 4 h, 8 h, and 12 h, respectively.

Firstly, for water-soaked Co-Ci-2D samples for 2 h, 4 h, 8 h, and 12 h, their TGA curves show the overlapped profiles, especially before 300 °C. Secondly, no obvious weight losses are found upon further heating to 75 °C: two consecutive weight loss appears in the range of 76-190 °C, corresponding to the release of coordinated water molecules. The total weight losses are 15.23%, 15.31%, 15.16% and 15.09% for 2 h, 4 h, 8 h, and 12 h, respectively. Specifically, the fist weigh losses for 2 h, 4 h, 8 h, and 12 h are 5.28%, 5.53%, 5.77% and 4.74%, respectively, resulting from the loss of Co-Ci-mono-B. The corresponding second weight losses are 9.95%, 9.78%, 9.39% and 10.35%, respectively, belonging to that of Co-Ci-mono-A. Finally, the weight ratios of Co-Ci-mono-A and Co-Ci-mono-B calculated from TGA curves are about 1.88/1, 1.77/1, 1.63/1 and 2.18/1 for 2 h, 4 h, 8 h, and 12 h, signifying that Co-Ci-mono-A is a main product for all their water-treated sample. Taken together, TGA results indicated that there are the analogical compositions in all their water-soaked samples.

Water-treated Ni-Ci-2D samples for 2 h, 4 h, 8 h, and 12 h shows the results similar to the corresponding Co-Ci-2D samples. It should be pointed out that the total weight

losses between 100 °C and 200 °C are 15.64%, 15.80%, 15.34% and 15.15% for 2 h, 4 h, 8 h, and 12 h, respectively. The first weight losses for 2 h, 4 h, 8 h, and 12 h are 3.83%, 4.10%, 4.07% and 3.90%, respectively, corresponding to the loss of Ni-Ci-mono-B (similar to the structure of Co-Ci-mono-B). The corresponding second weight losses are 11.81%, 11.70%, 11.27% and 11.25%, respectively, which are assigned to the loss of Ni-Ci-mono-A (similar to that of Co-Ci-mono-A). Similarly, the weight ratios of Ni-Ci-mono-A and Ni-Ci-mono-B measured from TGA curves are about 3.08/1, 2.85/1, 2.77/1 and 2.88/1 for 2 h, 4 h, 8 h, and 12 h, indicating that Ni-Ci-mono-A is a main product for all their water-treated sample.

· **IR spectra**

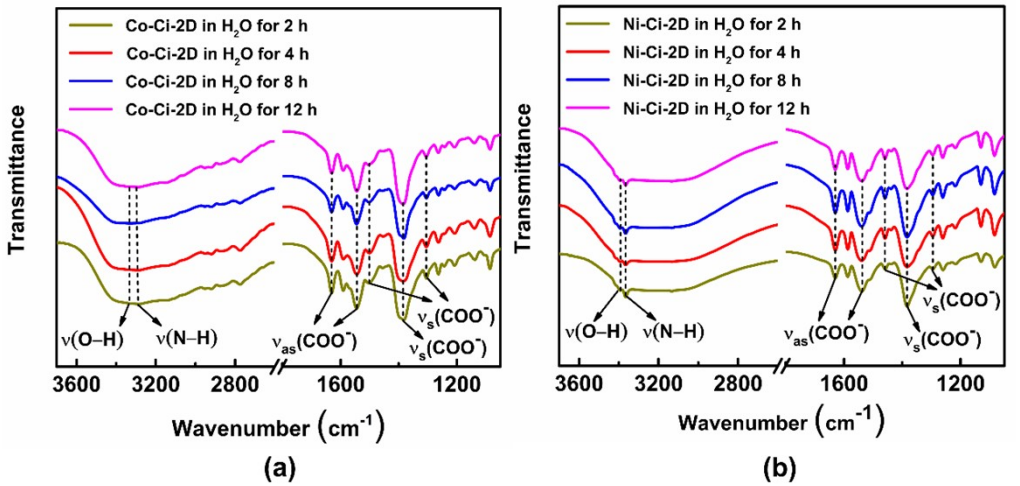

Fig. S15 IR absorption spectra of **Co-Ci-2D** (a) and **Ni-Ci-2D** (b) soaked in water for 2 h, 4 h, 8 h, and 12 h, respectively, in the solid state at room temperature.

It can be seen from Fig. S15 that water-soaked Co-Ci-2D samples for 2 h, 4 h, 8 h, and 12 h appears the same IR characteristic peaks, such as O−H and N−H stretching vibrations along with asymmetric and symmetric stretching vibrations of carboxylate group. The results shows that all water-soaked samples possess the similar chemical structures and compositions. Herein, the IR spectrum of Co-Ci-2D sample soaked in water for 2 h is served as a representative example and described in detail in the text.

Similarly, Ni-Ci-2D samples soaked in water for 2 h, 4h, 8h and 12h also display the almost identical IR peaks, suggesting the presence of similar chemical structures and compositions for all water-soaked samples. Due to the similarities of structure and composition, the IR spectrum of Ni-Ci-2D samples soaked in water for 2 h is discussed here representatively. It shows the O−H or N−H stretching vibrations from coordinated water molecules and ligand molecule at 3393 and 3365 cm^{-1}, respectively. A set of characteristic absorption bands are observed in the spectrum at 1629 and 1539 cm^{-1} along with 1458, 1383 and 1295 cm^{-1}, attributing to asymmetric stretching vibration and symmetric stretching vibration of carboxylate group, respectively. The

Δ values between $\nu_{as}(-COO^-)$ and $\nu_s(-COO^-)$ are 171, 156, 334 and 244 cm^{-1}, implying that there were ionic and monodentate modes in the mixture for carboxylate groups.

VIII. Characterization of Co-Ci-2D and Ni-Ci-2D treated by PBS solution

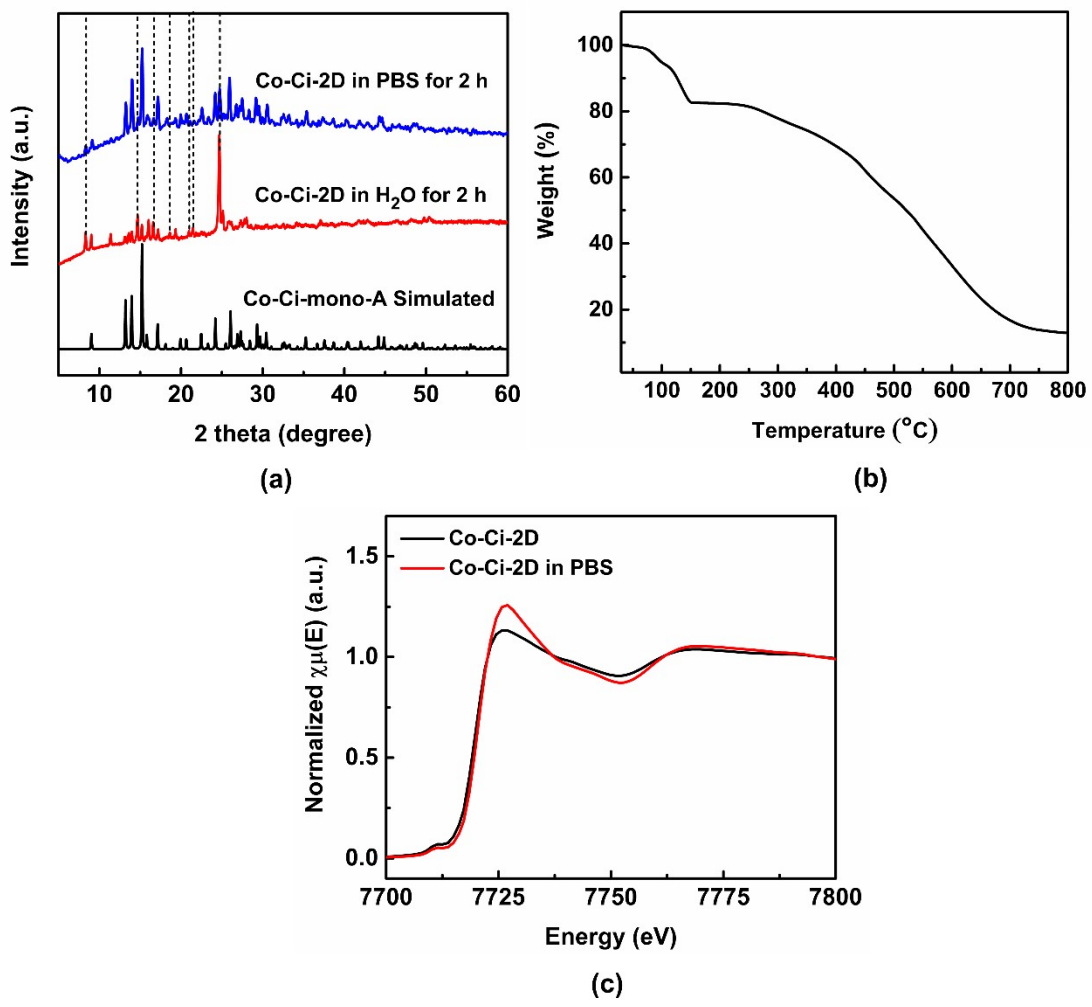

Fig. S16 Structural characterization of **Co-Ci-2D** soaked in the PBS solution for 2 h. (a) The PXRD patterns for **Co-Ci-mono-A** of a simulation based on single-crystal analysis and **Co-Ci-2D** soaked in water and the PBS solution for 2 h. (b) Thermogravimetric curve for **Co-Ci-2D** soaked in the PBS solution for 2 h. (c) Co K-edge XANES experimental spectra of **Co-Ci-2D** and **Co-Ci-2D** soaked in the PBS solution for 2 h.

For Co-Ci-2D, the sample soaked in the PBS solution for 2 h shows some peaks similar to Co-Ci-mono-A, the rest peaks match well with that of the water-soaked sample for 2 h, which is attributable to Co-Ci-mono-B. Furthermore, the TGA curve indicates that the total weight loss from 67 °C and 180 °C are 16.65% for the PBS-treated sample, corresponding to the removal of all coordinated water molecules. The result is close to the calculated weight loss of Co-Ci-mono-A (15.89 %) under the same condition, further suggesting that the above sample treated with the PBS solution had structure and composition analogical to Co-Ci-mono-A, belonging to a pair of isomers. Finally, X-ray absorption near-edge structure (XANES) spectrum of the PBS-treated Co-Ci-2D sample is very similar to that of the original Co-Ci-2D sample, suggesting that the PBS-treated and original Co-Ci-2D samples have the same coordination environment, an octahedral configuration. The well-remained coordination environment in the PBS-treated Co-Ci-2D sample further indicates that there is no formation of the non-coordinated compound and an analogical coordination structure in the mixture treated by the PBS solution. Taken together, the PBS-treated Co-Ci-2D sample should be made up of a pair of isomers, i.e. Co-Ci-mono-A and Co-Ci-mono-B, similar to the water-soaked Co-Ci-2D sample for 2 h.

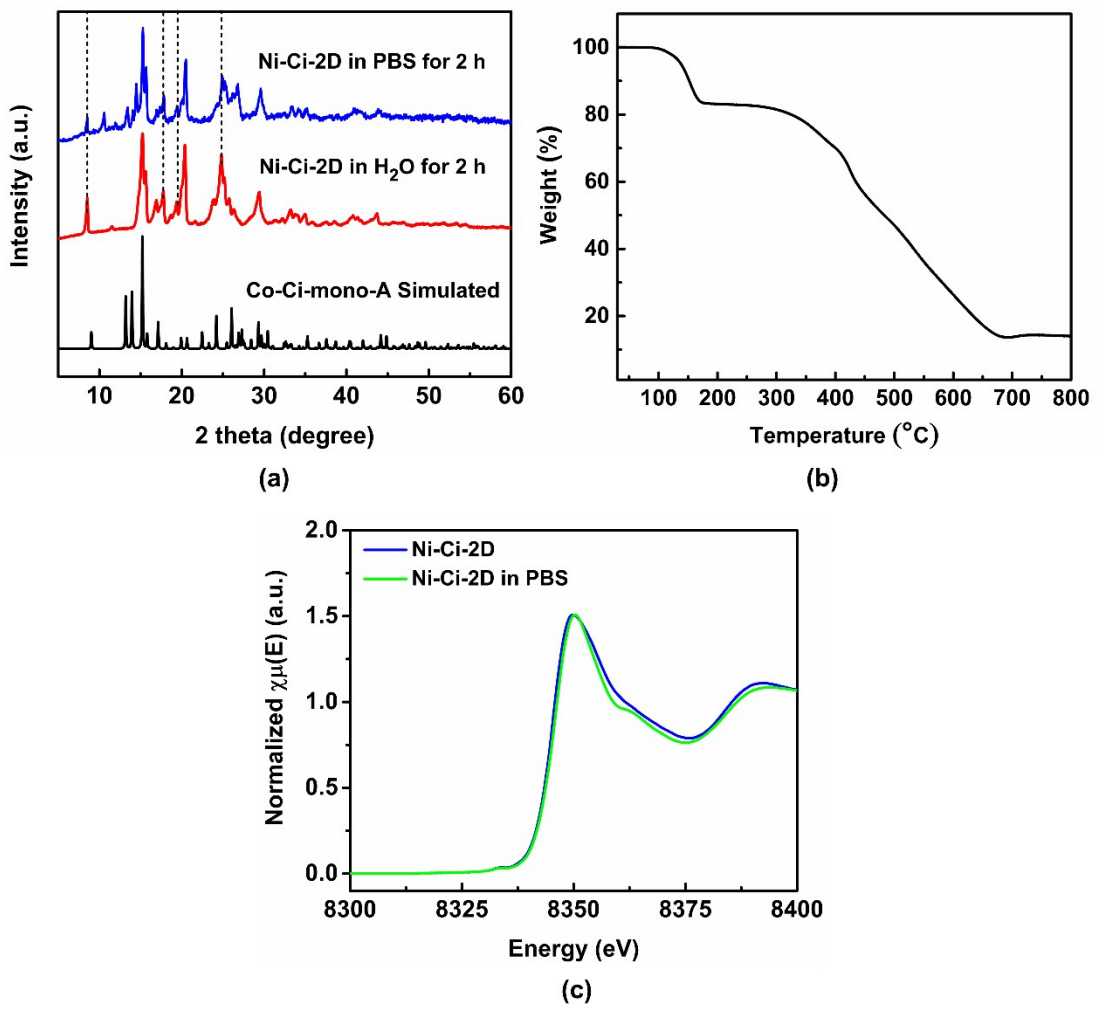

Fig. S17 Structural characterization of **Ni-Ci-2D** soaked in the PBS solution for 2 h. (a) The PXRD patterns for **Co-Ci-mono-A** of a simulation based on single-crystal analysis and **Ni-Ci-2D** soaked in water and the PBS solution for 2 h. (b) Thermogravimetric curve for **Ni-Ci-2D** soaked in the PBS solution for 2 h. (c) Co K-edge XANES experimental spectra of **Ni-Ci-2D** and **Ni-Ci-2D** soaked in the PBS solution for 2 h.

As shown in Fig. S17, some PXRD peaks observed in the PBS-treated Ni-Ci-2D sample for 2h are similar to the structure of Co-Ci-mono-A (i.e. isostructural Ni-Ci-mono-A), some peaks are consistent with that of Ni-Ci-mono-B found in a water-

soaked sample for 2 h, some peaks are undetected in the water-soaked Ni-Ci-2D sample. The undetected peaks are possibly ascribed to Ni-Ci-mono-B because the differently preferred orientation of the powder samples could lead to the omission of some peaks. The conclusion that the PBS-treated sample contains a pair of isomers, Ni-Ci-mono-A and Ni-Ci-mono-B, are also further confirmed by TGA and XANES measurements. The TGA result shows that the total weight loss of 16.72 % occurs in the temperature of 84-190 °C for the above sample, being equivalent to the theoretical weight loss of Ni-Ci-mono-A (15.90 %). This indicates that the PBS-treated Ni-Ci-2D sample contains compounds with the same molecular formula, which might be isomeric Co-Ci-mono-A and Co-Ci-mono-B. Moreover, the same XANES profiles are detected in the pristine and PBS-treated Ni-Ci-2D samples, implying that the two aforementioned samples have the similar octahedral coordination geometry. That is to say, the coordination environment of the PBS-treated Ni-Ci-2D sample does not change significantly, which is merely water molecules to participate in the reaction via the cleavage of the Ni−N or Ni−O bonds and form new compounds. Thus, the PBS-treated sample has the similar molecular composition, belonging to isomeric compounds, which is similar to the water-soaked Ni-Ci-2D sample for 2 h.

.

IX. XPS results of Co-Ci-2D and Ni-Ci-2D measured before and after OER tests

· **XPS survey**

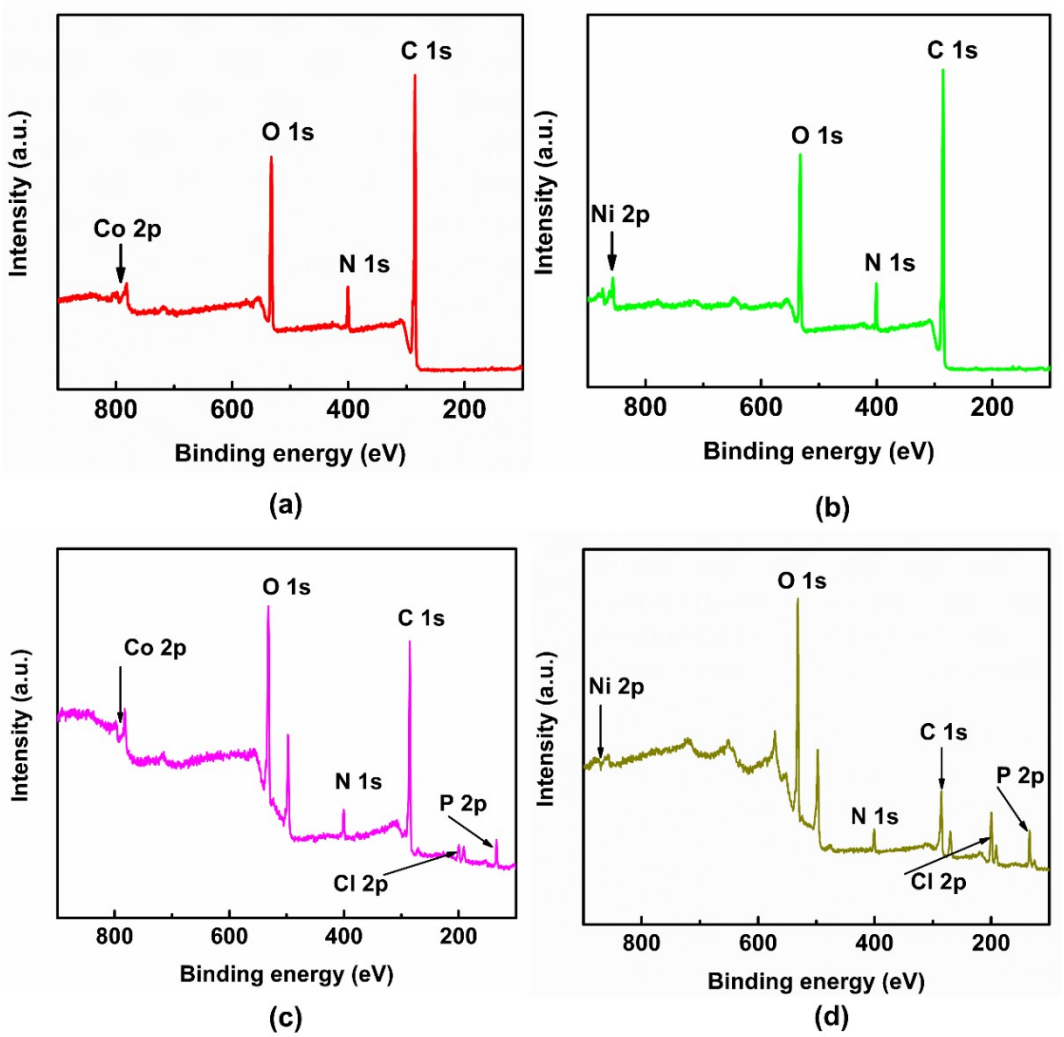

Fig. S18 XPS survey spectra of **Co-Ci-2D** measured before (a) and after (c) OER test. XPS survey spectra of **Ni-Ci-2D** measured before (b) and after (d) OER test.

The peaks of C 1s, O 1s, N 1s and Co 2p / Ni 2p are detected in the XPS survey spectra (Fig. S18), confirming the existence of the existence of C, O, N, Co elements

and C, O, N, Ni elements in fresh and used Co-Ci-2D and Ni-Ci-2D samples, respectively.

· **Comparison of deconvoluted peaks**

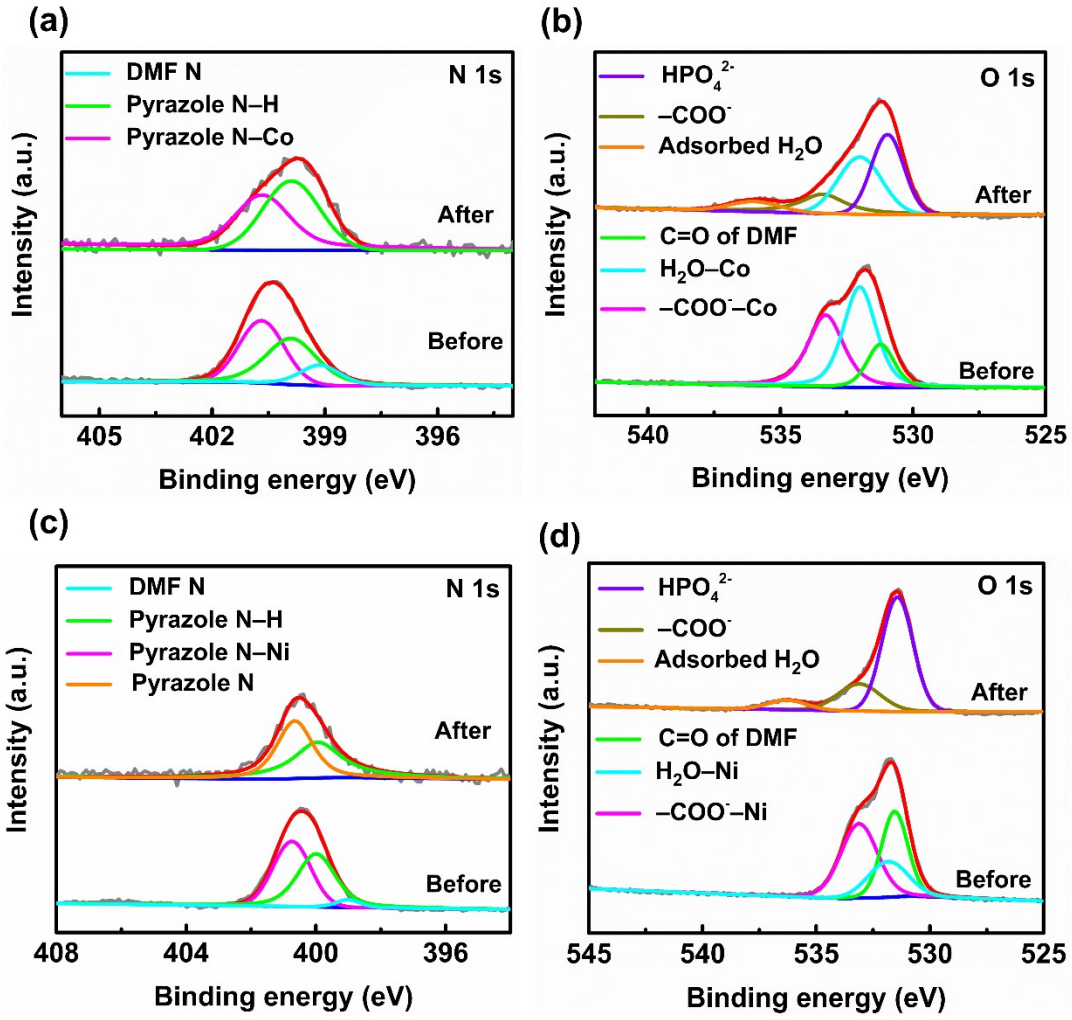

Fig. S19 High-resolution XPS spectra of N 1s (a) and O 1s (b) regions for Co-Ci-2D before and after OER. High-resolution XPS spectra of N 1s (c) and O 1s (d) regions for Ni-Ci-2D before and after OER.

For Co-Ci-2D, its N 1s XPS spectrum can be fitted by three different components, i.e., coordinated pyrazole nitrogen (Co–N, 400.7 eV), uncoordinated pyrazole nitrogen (N–H, 399.9 eV) and nitrogen atom from DMF molecule (399.2 eV) (Fig. S19a).[3] The high-resolution XPS spectrum of O 1s can be split into three energy peaks at 531.2, 532.0, and 533.3 eV (Fig. S19b), corresponding to the formyl group

(=C=O) from DMF molecule, coordinated H_2O molecules (H_2O–Co) and the carboxylate group (–COO^-–Co). [4, 5] Like Co-Ci-2D, the high-resolution spectra of N 1s, and O 1s in Ni-Ci-2D also shows the same deconvoluted peaks ((Fig. S19c, S19d and Table S4).

After OER, the high-resolution N 1s spectrum of Co-Ci-2D can be deconvoluted into Co–N and N–H species (Fig. S19a). Some obvious differences are found in the O1s spectra after OER (Fig. S19b), where deconvoluted peaks of O changes into coordinated H_2O molecules (532.0 eV), uncoordinated carboxylate group (533.4 eV), HPO_4^- from the PBS solution (531.0 eV) and adsorbed H_2O (536.1 eV).[4, 6] The alterations of deconvoluted N 1s and O 1s spectra demonstrates that a structural transformation of Co-Ci-2D occurred in the OER procedure. The unchanged Co 2p spectrum and more coordinated H_2O molecules relative to the carboxylate group in deconvoluted O 1s spectrum indicates that only water molecules participate in the cleavage reaction of Co−N or Co−O bonds to make Co-Ci-2D to change into mono coordination compounds, which is consistent with PXRD results after the OER reaction. Similar to treated Co-Ci-2D samples, the deconvoluted N 1s and O 1s spectra after OER are observed in treated Ni-Ci-2D (Fig. S19c and S19d), indicating that original organic ligands are retained in the measured sample.

Table S4 Comparison of deconvoluted peaks of Co 2p / Ni 2p, O 1s, N 1s and P 2p in the XPS spectra for **Co-Ci-2D**, **Ni-Ci-2D** before and after OER reaction for 2 h.

	Co-Ci-2D before OER	Co-Ci-2D After OER	Ni-Ci-2D before OER	Ni-Ci-2D After OER
Co/Ni 2p（eV）	$2p_{3/2}$: 781.4 Satellite: 785.6 $2p_{1/2}$: 797.1 Satellite: 803.4	$2p_{3/2}$: 781.5 Satellite: 786.3 $2p_{1/2}$: 797.2 Satellite: 803.6	$2p_{3/2}$: 856.1 Satellite: 862.1 $2p_{1/2}$: 873.6 Satellite: 880.1	$2p_{3/2}$: 856.7 Satellite: 860.2 $2p_{1/2}$: 874.5 Satellite: 800.7
N 1s（eV）	DMF N: 399.2 Pyrazole N–H: 399.9 Pyrazole N–Co: 400.7	Pyrazole N–H: 399.9 Pyrazole N–Co: 400.7	DMF N: 399.0 Pyrazole N–H: 399.98 Pyrazole N–Ni: 400.78	Pyrazole N–H: 399.98 Pyrazole N: 400.68
O 1s（eV）	C=O of DMF: 531.2 H_2O–Co: 532.0 $–COO^-$–Co: 533.3	HPO_4^-: 531.0 H_2O–Co: 532.0 $–COO^-$: 533.4 Adsorbed H_2O: 536.1	C=O of DMF: 531.6 H_2O–Ni: 531.8 $–COO^-$–Ni: 533.1	HPO_4^-: 531.4 $–COO^-$: 533.1 Adsorbed H_2O: 536.3
P 2p（eV）	Absent	$2p_{3/2}$: 133.0 $2p_{1/2}$: 134.2	Absent	$2p_{3/2}$: 133.2 $2p_{1/2}$: 134.5

X. Summary of characterization results of Co-Ci-2D and Ni-Ci-2D treated by PBS solution and after OER

Table S5 Summary of characterization results obtained from PXRD, TGA, XPS and XAS for PBS-treated **Co-Ci-2D** and **Ni-Ci-2D** along with **Co-Ci-2D** and **Ni-Ci-2D** after OER.

	PBS-treated Co-Ci-2D	Co-Ci-2D after OER for 2 h	PBS-treated Ni-Ci-2D	Ni-Ci-2D after OER for 2 h
PXRD result	Co-Ci-mono-A, Co-Ci-mono-B	Co-Ci-mono-A	Ni-Ci-mono-A, Ni-Ci-mono-B	Ni-Ci-mono-A
TGA result	a pair of isomers, Co-Ci-mono-A is major	–	a pair of isomers, Ni-Ci-mono-A is major	–
XPS result	–	a structural transformation from Co-Ci-2D to a mononuclear coordination compound	–	$NiHPO_4$
XANES result	well-remained octahedral configuration, no formation of non-coordinated compound	–	unchanged coordination environment, no formation of non-coordinated compound	partial unchanged coordination environment, partial $NiHPO_4$ signal
Real components	Co-Ci-mono-A, Co-Ci-mono-B	Co-Ci-mono-A	Ni-Ci-mono-A, Ni-Ci-mono-B	Ni-Ci-mono-A, $NiHPO_4$
Active species (The whole OER process)	Co-Ci-mono-A and Co-Ci-mono-B		Ni-Ci-mono-A, Ni-Ci-mono-B and $NiHPO_4$	

XI. Characterization of Co-Ci-2D and Ni-Ci-2D after pretreatment

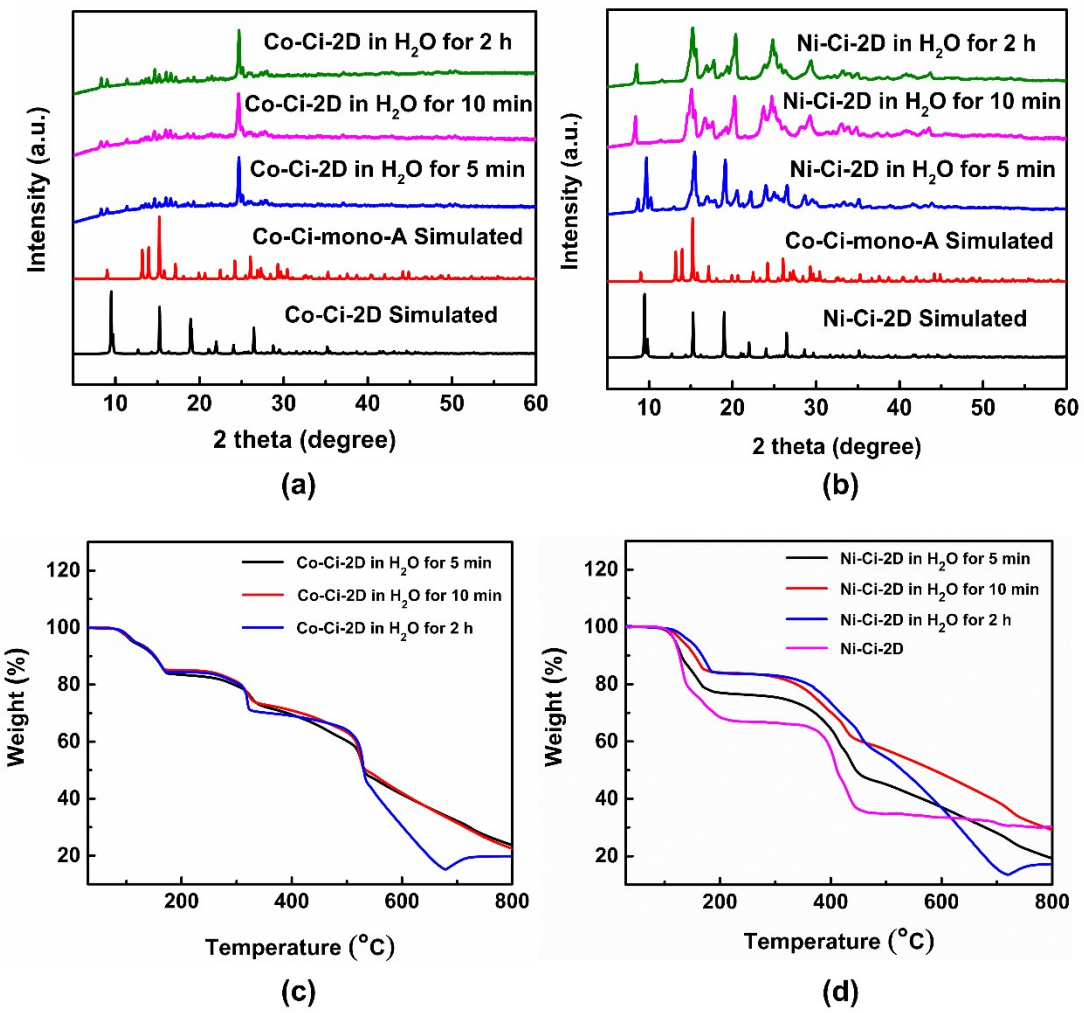

Fig. S20 (a) The PXRD patterns for **Co-Ci-2D and Co-Ci-mono-A** of a simulation based on single-crystal analysis and for **Co-Ci-2D** soaked in water for 5 min, 10 min and 2 h. (b) The PXRD patterns for **Ni-Ci-2D and Co-Ci-mono-A** of a simulation based on single-crystal analysis and for **Ni-Ci-2D** soaked in water for 5 min, 10 min and 2 h. (c) Thermogravimetric curves for **Co-Ci-2D** soaked in water for 5 min, 10 min and 2 h, respectively. (d) Thermogravimetric curves for **Ni-Ci-2D** and **Ni-Ci-2D** soaked in water for 5 min, 10 min and 2 h, respectively.

In order to measure electrocatalytic performance, the as-synthesized MOFs firstly need to add foreign water to form a homogenous ink under sonication. In the preparation process (i.e. within 10 min), these MOFs could probably react with water to generate new compounds. To corroborate the hypothesis, the samples of Co-Ci-2D and Ni-Ci-2D were immersed in water for 5 min and 10 min to simulate the time for the preparation. After being soaked in water for 5 min and 10 min, we measured the PXRD patterns of the above samples. As shown in Fig. S20a, the PXRD patterns of the water-soaked Co-Ci-2D samples for 5 min and 10 min are almost identical to that of the water-soaked Co-Ci-2D sample for 2 h, signifying that Co-Ci-2D rapidly converted into new compounds (Co-Ci-mono-A and Co-Ci-mono-B) within a short time. For Ni-Ci-2D, its PXRD pattern was changed after 5 min of water-soaking (Fig. S20b). Specifically, some peaks are similar to that of the simulated Ni-Ci-2D, some peaks are in accordance with the result simulated from Co-Ci-mono-A (i.e. isostructural Ni-Ci-mono-A). The result shows that Ni-Ci-2D did not completely transformed into new compounds and a part of Ni-Ci-2D remained intact within 5 min of water treatment. For the Ni-Ci-2D sample treated with water for 10 min (Fig. S20b), its PXRD pattern is the same as that of the water-treated Ni-Ci-2D sample for 2 h, suggesting that Ni-Ci-2D was completely turned into Ni-Ci-mono-A and Ni-Ci-mono-B at the end of 10 min. Additionally, the reaction rate to form new compounds between Co-Ci-2D and water (5 min) is faster than that between Ni-Ci-2D and water (10 min), which evidences the higher reactivity of Co-Ci-2D than that of Ni-Ci-2D.

Furthermore, the structural transformation of the water-soaked samples in a short time was confirmed by TGA. As shown in Fig. S20c, water-immersed Co-Ci-2D samples for 5 min, 10 min and 2 h show the similar curves before 300 °C, and their total weight losses are also very similar between 76 °C and 190 °C, being 16.08%, 14.55% and 15.23%, respectively. This indicates that these samples have the analogical compositions, i.e. the structure change was accomplished in the water-soaked Co-Ci-2D samples within a short time. Differently, a weight loss of 23.59% from 80 °C to 250 °C is observed in water-treated Ni-Ci-2D sample for 5 min, which

is smaller than that of Ni-Ci-2D (33.06%) and larger than that of the Ni-Ci-2D sample immersed in water for 2 h (15.64%). The result further testifies that there is an incompletely structural transformation in the water-treated Ni-Ci-2D sample for 5 min. For the Ni-Ci-2D sample soaked in water for 10 min, its weight loss (15.77%) and curve are analogous to that of 2 h in the range of 100–200 °C, indicating a completely structural alteration in the measured sample.

Notably, the results of PXRD measurement and TGA curves are in good agreement with each other, indicating that Co-Ci-2D and Ni-Ci-2D have decomposed into Co-Ci-mono-A and Co-Ci-mono-B, as well as Ni-Ci-mono-A and Ni-Ci-mono-B, respectively, within a very short time, i.e. 10 min. Because the immersed time of the sample in this experiment corresponds to the time of the catalyst ink preparation (within 10 min). In other words, the active species could probably form after the successful preparation of ink or before electrocatalytic OER rather than in the OER process.

Finally, one can see that the Co-Ci-2D samples soaked in water for 10 min and 2 h as well as treated with the PBS solution for 2 h show the similar results, forming new compounds of Co-Ci-mono-A and Co-Ci-mono-B due to water-triggered structural transformation of MOFs. The Ni-Ci-2D sample is analogous to that of the Co-Ci-2D sample, namely Ni-Ci-mono-A and Ni-Ci-mono-B. These new compounds act as active species to catalyze the OER under neutral condition.

XII. Comparison of OER performances in 0.1 M PBS solution

Table S6 Comparison of OER catalytic performance of **Co-Ci-2D, Ni-Ci-2D, IrO_2** and recently reported electrocatalysts working in 0.1 M PBS solution. The OER activities inferior and comparable to that of **Co-Ci-2D** were highlighted in yellow.

Catalysts	Mass loading (g cm^{-2})	Substrate	Onset potential (V vs. RHE)	η (1 mA cm^{-2}) (mV)	J (1.8 V) (vs. RHE, mA cm^{-2})	Tafel slop (mV dec^{-1})	Reference
Co-Ci-2D	0.283	GC	1.673	480 520 (2 mA cm^{-2})	3.93	165	This work
Ni-Ci-2D	0.283	GC	1.720	570 (0.34 mA cm^{-2})	0.34	215	This work
IrO_2	0.283	GC	1.632	410 490 (2 mA cm^{-2})	7.59	113	This work
FJU-82-Co	N/A	GC	N/A	570	1	571	2
Co-DP-MP@NCF	N/A	GC	1.531	N/A	2.5	129	7
2D-Co-MOF	0.714	Pyrolytic graphite	1.73	548 (2 mA cm^{-2})	N/A	88	8
NiFe-Pi	N/A	Nickel foam	N/A	495	4.45	N/A	9
$\{[Co_3(pyz)(fa)_3(dmso)_2]\cdot 2H_2O\}_n$	0.057	FTO	N/A	257	N/A	80.5	10
Co-B_i NS/G	0.283	GC	1.465	500 (10 mA cm^{-2})	14.4	160	11
Co-B_i NS	0.283	GC	1.596	N/A	5.3	274	11
Au-$Co(OH)_2$	N/A	FTO	1.513	410	1.6	370	12
Co_3S_4 ultrathin nanosheet	0.28	GC	1.54	700 (3.97 mA cm^{-2})	2.4	151	13
Co_3O_4/SWNTS	0.05	FTO	1.70	450	6	104	14
$LiCoPO_4$	0.1	GC	1.60	N/A	0.5	120	15
Co-P_i	1±0.1	Ni foam	1.61	N/A	0.57	N/A	16
Co_3O_4	1±0.1	Ni foam	1.64	N/A	0.61	N/A	16

Fe-based film HEPES	12.3 nmol cm^{-2}	ITO	1.703	473	5.1	47	17
ZrS_3 nanosheet	N/A	ITO	1.84	N/A	0.025	102	18
ZIF-67	0.22	GC	1.628	525 (2 mA cm^{-2})	N/A	127	19
MOF-74-Co	0.22	GC	1.613	492 (2 mA cm^{-2})	4.9	134	19
Fe_3-Co_2	0.22	GC	1.529	431 (2 mA cm^{-2})	8.8	129	19
MAF-6-Co	0.2	GC	1.664	559 (2 mA cm^{-2})	2.2	215	20
Co4Mo	0.2	GC	1.500	388 (2 mA cm^{-2})	22.0	144	20
Co4W	0.2	GC	1.595	482 (2 mA cm^{-2})	4.9	178	20
Cu-doped CCO	N/A	FTO	1.78	653	N/A	N/A	21
$ZnCo_2O_4$	N/A	Pt-Ti	N/A	480	N/A	76	22
Fe-based Film	10.2 nmol cm^{-2}	ITO	N/A	480	N/A	N/A	23
Co-TpBpy	N/A	GC	ca. 1.630	400	19.5	59	24
Au/Co_3O_4	N/A	GC	1.61	650 (10 mA cm^{-2})	6.1	N/A	25
A-$Co_{4.6}O_{0.6}P$ NCs	0.8	GC	1.5	400	4.59	164	26
Co/CoP-5	0.88	GC	N/A	500	2.6	N/A	27
$CuCo_2O_4$/ Nr GO	0.14	GC	N/A	1150 (10 mA cm^{-2})	N/A	N/A	28
Co-Ni-LDHs	0.17 μg cm^{-2}	FTO	1.623	490	N/A	N/A	29
Co/Fe	N/A	FTO	1.59	510	N/A	111	30
CoHCF	1.4±0.2 μg cm^{-2}	FTO	1.51	400	N/A	85	31
Co_3O_4 micelle	3	FTO	N/A	410 (0.5 mA cm^{-2})	N/A	N/A	32
CoHCF film	N/A	Carbon paper	N/A	470	N/A	N/A	33
Surface-oxidized stainless steel SO330	N/A	Stainless steel	N/A	502 (0.65 mA cm^{-2})	N/A	N/A	34
Mncat	98 nmol cm^{-2}	ITO	N/A	590	N/A	76	35

Note:

N/A: Not Applicable.

GC: glassy carbon.

FTO: fluorine-doped tin oxide glass.

Pt-Ti: Pt-Ti alloy coated glass.

ITO: indium tin oxide.

XIII. Reference for Supporting Information

1 J. Li, W. Huang, M. Wang, S. Xi, J. Meng, K. Zhao, J. Jin, W. Xu, Z. Wang, X. Liu, Q. Chen, L. Xu, X. Liao, Y. Jiang, K. A. Owusu, B. Jiang, C. Chen, D. Fan, L. Zhou and L. Mai, *ACS Energy Lett.*, 2019, 4, 285−292.

2 M. Zhang, Q. Lin, W. Wu, Y. Ye, Z. Yao, X. Ma, S. Xiang and Z. Zhang, *ACS Appl. Mater. Interfaces*, 2020, **12**, 16367−16375.

3 X. Sang, X. Hu, R. Tao, Y. Zhang, H. Zhu and D. Wang, *ChemPlusChem*, 2020, **85**, 123–129.

4 J. Jiang, L. Huang, X. Liu and L. Ai, *ACS Appl. Mater. Interfaces*, 2017, **9**, 7193−7201.

5 Y. J. Kim and C. R. Park, *Inorg. Chem.*, 2002, 41, 6211–6216.

6 Q. Qin, H. Jang, P. Li, B. Yuan, X. Liu and J. Cho, *Adv. Energy Mater.*, 2020, **9**, 1803312.

7 J. Saha, S. Verma, R. Ball, C. Subramaniam and R. Murugavel, *Small*, 2019, **16**, 1903334.

8 S. Gutiérrez-Tarriño, J. L. Olloqui-Sariego, J. J. Calvente, G. M. Espallargas, F. Rey, A. Corma and P. Oña-Burgos, *J. Am. Chem. Soc.*, 2020, **142**, 19198–19208.

9 G. Givirovskiy, V. Ruuskanen, T. Väkiparta and J. Ahola*, Mater. Today Energy*, 2020, **17**, 100426.

10 S. Ibrahim, K. Shehzadi, B. Iqbal, S. Abbas, D. R. Turner and M. A. Nadeem, *J. Colloid and Inter. Sci.*, 2019, **545**, 269–275.

11 P. Chen, K. Xu, T. Zhou, Y. Tong, J. Wu, H. Cheng, X. Lu, H. Ding, C. Wu and Y. Xie, *Angew. Chem. Int. Ed.*, 2016, **55**, 2488–2492.

12 Y. Zhang, B. Cui, Z. Qin, H. Lin and J. Li, *Nanoscale*, 2013, **5**, 6826–6833.

13 Y. Liu, C. Xiao, M. Lyu, Y. Lin, W. Cai, P. Huang, W. Tong, Y. Zou and Y. Xie, *Angew. Chem. Int. Ed.*, 2015, **127**, 11383–11387.

14 J. Wu, Y. Xue, X. Yan, W. Yan, Q. Cheng and Y. Xie, *Nano Res.*, 2012, **5**, 521–530.

15 S. W. Lee, C. Carlton, M. Risch, Y. Surendranath, S. Chen, S. Furutsuki, A. Yamada, D. G. Nocera, Y. Shao-Horn, *J. Am. Chem. Soc.*, 2012, **134**, 16959–16962.

16 H. S. Ahn and T. D. Tilley, *Adv. Funct. Mater.*, 2013, **23**, 227–233.

17 M. Chen, Y. Wu, Y. Han, X. Lin, J. Sun, W. Zhang and R. Cao, *ACS Appl. Mater. Interfaces*, 2015, **7**, 21852−21859.

18 J. Xie, R. Wang, J. Bao, X. Zhang, H. Zhang, S. Li and Y. Xie, *Inorg. Chem. Front.*, 2014, **1**, 751–756.

19 J. -Q. Shen, P. -Q. Liao, D. -D. Zhou, C. -T. He, J. -X. Wu, W. -X. Zhang, J. -P. Zhang and X. -M. Chen, *J. Am. Chem. Soc.*, 2017, **139**, 1778–1781.

20 Y. -T. Xu, Z. -M. Ye, J. W. Ye, L. M. Cao, R. K. Huang, J. X. Wu, D. -D. Zhou, X. -F. Zhang, C. -T. He, J. -P. Zhang and X. -M. Chen, *Angew. Chem. Int. Ed.*, 2019, **58**, 139–143.

21 Y. Zhang, B. Cui, O. Derr, Z. Yao, Z. Qin, X. Deng, J. Li and H. Lin, *Nanoscale*, 2014, **6**, 3376–3383.

22 T. W. Kim, M. A Woo, M. Regis and K. -S. Choi, *J. Phys. Chem. Lett.*, 2014, **5**, 2370−2374.

23 Y. Wu, M. Chen, Y. Han, H. Luo, X, M. -T. Zhang, X. Lin, J. Sun, L. Wang, L. Deng, W. Zhang and R. Cao, *Angew. Chem. Int. Ed.*, 2015, **54**, 4870–4875.

24 H. B. Aiyappa, J. Thote, D. Balaji Shinde, R. Banerjee and S. Kurungot, *Chem. Mater.*, 2016, **28**, 4375–4379.

25 X. Lu, Y. H. Ng and C. Zhao, *ChemSusChem*, 2014, **7**, 82–86.

26 P. Cai, J. Huang, J. Chen and Z. Wen, *Angew. Chem. Int. Ed.*, 2017, **56**, 4858–4861.

27 Z. -H. Xue, H. Su, Q. Y. Yu, B. Zhang, H. -H. Wang, X. -H. Li and J. -S. Chen, *Adv. Energy Mater*., 2017, **7**, 1602355.

28 S. K. Bikkarolla and P. Papakonstantinou, *J. Power Sources*, 2015, **281**, 243–251.

29 Y. Zhang, B. Cui, C. Zhao, H. Lin and J. Li, *Phys. Chem. Chem. Phys.,* 2013, **15**, 7363–7369.

30 M. Aksoy, S. V. K. Nune and F. Karadas, *Inorg. Chem.*, 2016, **55**, 4301–4307.

31 S. Pintado, S. Goberna-Ferrón, E. C. Escudero-Adán and J. R. Galán-Mascarós, *J. Am. Chem. Soc.*, 2013, **135**, 13270−13273.

32 P. W. Menezes, A. Indra, D. González-Flores, N. R. Sahraie, I. Zaharieva, M. Schwarze, P. Strasser, H. Dau and M. Driess, *ACS Catal.*, 2015, **5**, 2017–2027.

33 H. T. Bui, D. Y. Ahn, N. K. Shrestha, M. M. Sung, J. K. Lee and S. H. Han, *J. Mater. Chem. A*, 2016, **4**, 9781–9788.

34 H. Schäfer, S. M. Beladi-Mousavi, L. Walder, J. Wollschläger, O. Kuschel, S. Ichilmann, S. Sadaf, M. Steinhart, K. Küpper and L. Schneider, *ACS Catal.*, 2015, **5**, 2671–2680.

35 I. Zaharieva, P. Chernev, M. Risch, K. Klingan, M. Kohlhoff, A. Fischer and H. Dau, *Energy Environ. Sci.*, 2012, **5**, 7081–7089.